Two-center interference and stereo Wigner time delay in photoionization of asymmetric molecules

Yijie Liao,[1] Yueming Zhou,[1,*] Liang-Wen Pi,[2,3,†] Qinghua Ke,[1] Jintai Liang,[1] Yong Zhao,[1] Min Li,[1] and Peixiang Lu[1,4,5,‡]

[1]*School of Physics and Wuhan National Laboratory for Optoelectronics, Huazhong University of Science and Technology, Wuhan 430074, China*

[2]*State Key Laboratory of Transient Optics and Photonics, Xi'an Institute of Optics and Precision Mechanics of the Chinese Academy of Sciences, Xi'an 710119, China*

[3]*University of Chinese Academy of Science, Beijing 100049, China*

[4]*Hubei Key Laboratory of Optical Information and Pattern Recognition, Wuhan Institute of Technology, Wuhan 430205, China*

[5]*CAS Center for Excellence in Ultra-intense Laser Science, Shanghai 201800, China*

(Received 19 May 2021; accepted 9 July 2021; published 20 July 2021)

We present numerical simulations of the time delay in photoemission of asymmetric diatomic molecules using the technique of reconstruction of attosecond beating by interference of two-photon transitions (RABITT) by solving the time-dependent Schrödinger equation. Our results show an obvious time delay between photoelectrons emitted to the left and right and this relative time delay oscillates as the photoelectron energy changes. More interestingly, the amplitude of this oscillation increases when the asymmetry degree of diatomic molecules decreases. With the method of the selected continuum wave functions, we calculate the Wigner time delay in photoionization. The obtained stereo Wigner time delay also oscillates with photoelectron energy. This oscillation is traced back to two-center interferences and it could explain the relative time delay in the RABITT measurement. Furthermore, our results indicate that the continuum-continuum time delay in photoemission of heteronuclear molecules is asymmetric.

DOI: 10.1103/PhysRevA.104.013110

I. INTRODUCTION

Since the experimental demonstration of extreme ultraviolet (XUV) pulses with duration below the femtosecond scale [1,2], these attosecond pulses have become a unique tool to study the electronic dynamics inside atoms and molecules in their natural timescale. The techniques of attosecond streaking [3–7] and reconstruction of attosecond beating by interference of two-photon transitions (RABITT) [8–12] are two prevailing approaches to probing the ultrafast electronic dynamics utilizing attosecond pulses [13]. In the RABITT technique, an XUV attosecond pulse train (APT) synchronized with a weak time-delayed infrared (IR) field ionizes a target. The energy spectra of photoelectrons are recorded as a function of the relative delay between XUV and IR pulses, which consist of main peaks corresponding to absorption of a single XUV photon and sidebands related to absorption or emission of an additional IR photon. The amplitude of sideband signals is periodically modulated as the relative delay varies, from which the photoemission time delay can be extracted. Nowadays, the RABITT technique is extensively employed to measure the attosecond photoionization time delay in atoms [14–16], molecules [17–20], and solids [21–23].

The retrieved time delay in RABITT measurements, τ_R, is connected with the phase of two-photon dipole transition matrix elements [24–31] and could be approximately decomposed into three parts $\tau_R = \tau_{XUV} + \tau_W + \tau_{CC}$, where τ_{XUV} and τ_W are the group delay of the XUV field and the Wigner time delay [32,33] associated with the bound-free transition, respectively, and τ_{CC} is the measurement-induced time delay corresponding to the free-free (continuum-continuum) transition. The Wigner time delay τ_W is of particular interest since it reveals the target potential landscape. Over the years, the Wigner time delay has been deeply surveyed for a variety of atoms and molecules [27,28,34–44]. Apparent relative time delays have been revealed for photoelectrons ejected from different subshells of atoms [34–36,45–48]. The emission-angle dependence of the Wigner time delay in atoms has also been reported [37–39]. In molecules, owing to the lower symmetry degree of the molecular potential, the Wigner time delay presents a more complicate angular dependence [27,28,40]. In addition, the complexity of molecules triggers abundant phenomena in the photoemission time delay induced by shape resonances [41], the potential environment of functional groups [42], chiral asymmetries [43], and so on, which have aroused broad attention. Studying the photoionization of molecules builds a bridge between atomic photoemission and that from solids or surfaces [49–51].

In asymmetric molecules, the concept of self-referenced stereo Wigner time delay (SWTD) was proposed [40,52,53], which measures the relative delay between electrons emitted to the left and right of molecules. This quantity directly

*zhouymhust@hust.edu.cn
†lwpi@opt.ac.cn
‡lupeixiang@hust.edu.cn

accesses the Wigner time-delay difference and it is sensitive to asymmetries of the molecule. In previous studies [40], the scheme of SWTD has been employed to follow the intramolecular photoemission dynamics of CO on the attosecond timescale and an obvious left-right relative time delay in RABITT measurements has been observed. This relative time delay was interpreted as the consequence of an asymmetry in the initial location of an ionized photoelectron wave packet (PEWP) with respect to the molecular geometric center [40]. This intuitive interpretation is valid for molecules with extreme asymmetries, for which it is a good approximation that the ionized electron wave packet launches from one side of the diatomic molecule. Generally, in photoionization of diatomic molecules, PEWPs launch from both nuclei and thus the interference occurs in the photoelectron spectra [54]. This two-center interference greatly affects the Wigner time-delay characteristics [55]. For example, in the homonuclear diatomic molecule $H_2{}^+$, it has been demonstrated that the two-center interference in photoemission dramatically increases the magnitude of the Wigner time delay and it could lead to either positive and negative time delays [56]. In addition, the two-center interference in $H_2{}^+$ leads to different behaviors of the angle-resolved time delay, compared with the He^+ atom [57]. In heteronuclear molecules, the PEWPs from two molecular nuclei have nonequivalent amplitudes, leading to different two-center-interference effects on the magnitude of the Wigner time delay. In particular, the amplitude ratio of two PEWPs is relevant to the asymmetry degree of diatomic molecules. It is worthwhile to survey the photoionization time delay in heteronuclear molecules and reveal the two-center-interference effect on the magnitude of the time delay in these asymmetric molecules.

In this paper we systematically study the time delays in photoemission of asymmetric diatomic molecules utilizing the RABITT technique. In particular, we focus on the left-right asymmetry of the time delay in heteronuclear molecules. Our results show that both the left-right relative RABITT time delay and the left-right relative Wigner time delay fluctuate as a function of photoelectron energy and the amplitudes of these fluctuations depend on the asymmetry degree of diatomic molecules. These fluctuations in the relative time delays are attributed to the interference between the electron wave packets launching from two molecular nuclei. Furthermore, the details of the fluctuations in the relative RABITT time delay and the relative Wigner time delay are different. This difference indicates the left-right asymmetric continuum-continuum (CC) time delay in photoionization of heteronuclear molecules.

This paper is structured as follows. In Sec. II we introduce the numerical methods, including solving the time-dependent Schrödinger equation (TDSE) in Sec. II A, extracting the time delay in RABITT measurements in Sec. II B, and the calculation of the Wigner time delay with the selected continuum wave function (SCWF) method [58] in Sec. III C. The RABITT time-delay results are shown in Sec. III A and the Wigner time-delay results are exhibited in Sec. III B. The CC time-delay results are discussed in Sec. III C. We finish with a summary in Sec. IV. Atomic units will be used throughout this paper unless otherwise stated.

II. NUMERICAL METHODS

A. One-dimensional time-dependent Schrödinger equation

To demonstrate the effect of two-center interferences on the time delay in photoionization of diatomic molecules, we perform numerical simulations in a one-dimensional (1D) model, which has been employed to study the time delay for the diatomic molecule CO with the scheme of attosecond streaking [52]. This 1D model is very simple but is valid and effective in demonstrating the underlying physics. We solve the TDSE for diatomic molecules within the single-active-electron approximation

$$i\frac{\partial}{\partial t}\Psi(x,t) = [\hat{H}_0 + \hat{H}_{\rm int}(t)]\Psi(x,t), \tag{1}$$

where $\hat{H}_{\rm int}(t)$ describes the interaction with external fields. Here the external APT (with a field intensity of $5\times 10^{14}{\rm W/cm^2}$) and the IR field (with a field intensity of $3\times 10^{10}{\rm W/cm^2}$ and a duration of 21 fs) are linearly polarized, with their common polarization axis parallel to the molecular axis. Here $\hat{H}_0 = -\frac{1}{2}\frac{\partial^2}{\partial x^2} + V(x)$ is the Hamiltonian of the field-free target. The target potential is given as

$$V(x) = -\frac{Z_L}{\sqrt{1+\left(x+\frac{R_0}{2}\right)^2}} - \frac{Z_R}{\sqrt{1+\left(x-\frac{R_0}{2}\right)^2}}, \tag{2}$$

where $R_0 = 4.0$ a.u. is the internuclear distance of molecules. In addition, $Z_{L\,(R)}$ is the charge of the left (right) molecular nucleus, with the charge ratio $\frac{Z_L}{Z_R}$ characterizing the asymmetry degree of molecules. In particular, $\frac{Z_L}{Z_R}\to 0$ corresponds to an extremely asymmetric molecule and $\frac{Z_L}{Z_R}=1$ matches a symmetric molecule. Here the nuclear charges (Z_L, Z_R) change from (0.0,1.0) to (0.5,0.5), satisfying $Z_L + Z_R = 1$.

In our calculation, the grid size is 4000 a.u. with a spacing $\Delta x = 0.1$ a.u. The ground states are obtained using imaginary-time propagation, yielding the ionization potentials $I_p = 0.67$, 0.62, 0.57, 0.53, 0.49, and 0.47 a.u. for $(Z_L, Z_R) = (0.0, 1.0)$, (0.1,0.9), (0.2,0.8), (0.3,0.7), (0.4,0.6), and (0.5,0.5), respectively. We implement the split-operator method [59] to solve the TDSE with a time step $\Delta t = 0.05$.

B. Data analysis in RABITT measurements

Ionization amplitudes are obtained by solving the TDSE. Squared ionization amplitudes give the photoelectron energy spectrum. We separately collect the energy spectra of photoelectrons emitted to the left (with negative momenta) and right (with positive momenta). In the photoelectron spectra, the yield of sidebands (SBs) oscillates with the relative delay τ between the XUV and IR fields [26]

$$S_{2q} = \alpha + \beta\cos[2\omega(\tau - \tau_R)], \tag{3}$$

where ω is the frequency of the IR field. Adopting the finite-difference approximation, the time delay in RABITT measurements can be expressed as

$$\begin{aligned}\tau_{\rm R} &= \frac{\Delta\phi_{\rm XUV}}{2\omega} + \frac{\Delta\eta}{2\omega} + \frac{\Delta\phi_{\rm CC}}{2\omega} \\ &= \tau_{\rm XUV} + \tau_{\rm W} + \tau_{\rm CC},\end{aligned} \tag{4}$$

with the IR probe frequency $\omega = 1.55$ eV. In our calculations, the group delay of the XUV pulses is zero and thus

$$\tau_{\mathrm{R}} = \tau_{\mathrm{W}} + \tau_{\mathrm{CC}}. \tag{5}$$

The oscillating sideband signals are integrated over an energy range of roughly 1.5 eV and fitted to Eq. (3) after being frequency filtered by a Fourier transform [40].

C. The SCWF method

The Wigner time delay τ_{W} is the term of most interest. We calculate τ_{W} using the SCWF method [58]. The SCWFs are real-valued functions for one-photon transitions [58], from which scattering phase shifts and the Wigner time delay can be retrieved. The scattering phase is extracted from the SCWFs with the Wronskian functional [60]. The Wigner time delay is the energy derivative of the scattering phase. Note that our calculation of the Wigner time delay with the SCWF method takes an atom potential as a reference, with its nucleus located at $x = 0$ a.u. This reference potential is modeled as

$$V_{\mathrm{ref}} = -\frac{1}{\sqrt{x^2 + a^2}}, \tag{6}$$

with $a = 1.3$, yielding the ground state with the ionization potential $I_p = 0.5$ a.u.

The scattering phase calculated by the SCWF method is defined as

$$\eta^{\text{left (right)}} \equiv \eta^{\text{left (right)}}_{\text{target}} - \eta_{\text{ref}}, \tag{7}$$

where $\eta^{\text{left (right)}}_{\text{target}}$ is the absolute scattering phase of photoelectrons emitted to the left (right), escaping through the target potential. In addition, η_{ref} is the absolute scattering phase of photoelectrons going through the reference potential, which is symmetric for photoelectrons emitted to the left and right.

Applying the finite-difference approximation, the Wigner time delay is

$$\tau_{\mathrm{W}}^{\text{left (right)}} \approx \frac{\eta^{\text{left (right)}}(E + \Delta E) - \eta^{\text{left (right)}}(E - \Delta E)}{2\Delta E}, \tag{8}$$

where the energy interval ΔE equals the IR frequency ω. The SWTD is defined as [52]

$$\tau_{\mathrm{SWTD}} \equiv \tau_{\mathrm{W}}^{\mathrm{left}} - \tau_{\mathrm{W}}^{\mathrm{right}}, \tag{9}$$

which measures the Wigner time-delay difference between photoelectrons emitted to the left and right of the target.

III. RESULTS AND DISCUSSION

A. Time delay in RABITT measurements

Figures 1(a) and 1(b) display the photoelectron energy spectra obtained by solving the TDSE, where the nuclear charges of the target are $(Z_L, Z_R) = (0.3, 0.7)$. Figures 1(a) and 1(b) correspond to the spectra of photoelectrons emitted to the left and right, respectively. The weak sidebands between the main peaks are clearly visible. The yield of each sideband oscillates with the relative delay τ between the XUV and IR fields. This oscillation encodes the information of photoionization time delay. Previous studies have reported that the photoionization time delays are different for the electrons emitted to the left and right sides of an asymmetric molecule

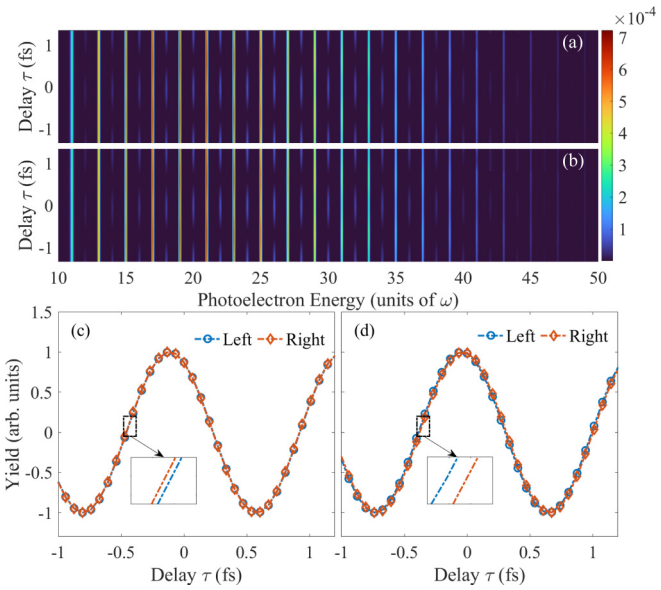

FIG. 1. (a) Energy spectrum of photoelectrons emitted to the left side of the diatomic molecule $[(Z_L, Z_R) = (0.3, 0.7)]$. (b) Same as in (a) but for photoelectrons emitted to the right side. (c) Yield of SB 12 as a function of the relative delay between the XUV and IR fields. The blue circles are the yield of photoelectrons emitted to the left and the orange rhombuses correspond to photoelectrons emitted to the right. The inset depicts a part of the magnified sideband signals. (d) Same as in (c) but for SB 20.

[40,52,53]. To reveal this difference, we compare the τ dependence of the yields of photoelectrons emitted to the left and right, as shown in Figs. 1(c) and 1(d). Indeed, there is a small shift between photoelectrons emitted to the two sides and this shift is energy dependent. For instance, the shift for SB 20 [Fig. 1(d)] is larger than that of SB 12 [Fig. 1(c)].

We extract the time delays for photoelectrons emitted to the left ($\tau_{\mathrm{R}}^{\mathrm{left}}$) and right ($\tau_{\mathrm{R}}^{\mathrm{right}}$) using Eq. (3), as displayed in Figs. 2(a)–2(f). Here the nuclear charges (Z_L, Z_R) change from (0.0,1.0) to (0.5,0.5). For the case $(Z_L, Z_R) = (0.0, 1.0)$, corresponding to an atom located at $x = 2.0$ a.u., the time delays $\tau_{\mathrm{R}}^{\mathrm{left}}$ and $\tau_{\mathrm{R}}^{\mathrm{right}}$ are exactly the same. This is because the photoelectron momentum distribution does not depend on where the ionized atom is located, and thus $\tau_{\mathrm{R}}^{\mathrm{left}}$ and $\tau_{\mathrm{R}}^{\mathrm{right}}$ are symmetric for this atomic potential. For the symmetric molecule with $(Z_L, Z_R) = (0.5, 0.5)$, as shown in Fig. 2(f), $\tau_{\mathrm{R}}^{\mathrm{left}}$ exactly coincides with $\tau_{\mathrm{R}}^{\mathrm{right}}$, as expected. As the photoelectron energy increases, $\tau_{\mathrm{R}}^{\mathrm{left}}$ and $\tau_{\mathrm{R}}^{\mathrm{right}}$ approach zero, which is quantitatively consistent with the results in [61]. For the asymmetric molecules, the difference between $\tau_{\mathrm{R}}^{\mathrm{left}}$ and $\tau_{\mathrm{R}}^{\mathrm{right}}$ is apparent, as displayed in Figs. 2(b)–2(e). For the case $(Z_L, Z_R) = (0.1, 0.9)$, as given in Fig. 2(b), $\tau_{\mathrm{R}}^{\mathrm{left}}$ and $\tau_{\mathrm{R}}^{\mathrm{right}}$ are nearly the same at photoelectron energies below 10 eV. At photoelectron energies ranging from 10 to 35 eV, $\tau_{\mathrm{R}}^{\mathrm{right}}$ is larger than $\tau_{\mathrm{R}}^{\mathrm{left}}$. As the asymmetry degree of molecules declines, the difference between $\tau_{\mathrm{R}}^{\mathrm{left}}$ and $\tau_{\mathrm{R}}^{\mathrm{right}}$ becomes more obvious. For the case $(Z_L, Z_R) = (0.4, 0.6)$, as shown in Fig. 2(e), $\tau_{\mathrm{R}}^{\mathrm{left}}$ is much smaller than $\tau_{\mathrm{R}}^{\mathrm{right}}$ at energies

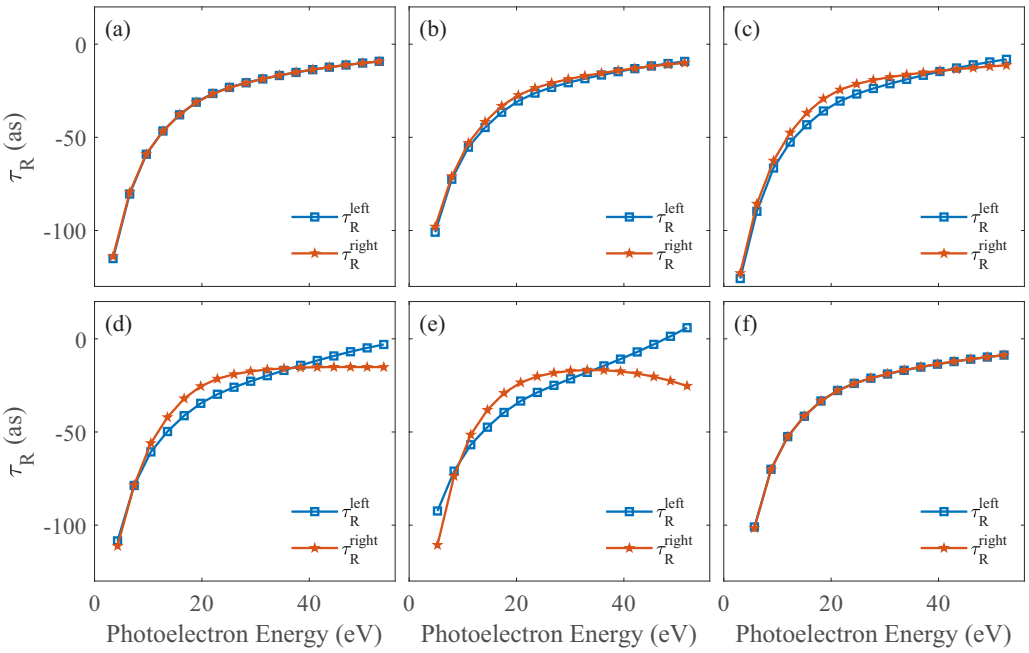

FIG. 2. The RABITT time delays in photoionization of different targets with nuclear charges of (a) $(Z_L, Z_R) = (0.0, 1.0)$, (b) $(Z_L, Z_R) = (0.1, 0.9)$, (c) $(Z_L, Z_R) = (0.2, 0.8)$, (d) $(Z_L, Z_R) = (0.3, 0.7)$, (e) $(Z_L, Z_R) = (0.4, 0.6)$, and (f) $(Z_L, Z_R) = (0.5, 0.5)$. The blue squares are the RABITT time delay of photoelectrons emitted to the left and the orange pentagrams correspond to photoelectrons emitted to the right.

ranging from 10 to 35 eV. At photoelectron energies above 35 eV, τ_R^{left} becomes much larger than τ_R^{right}.

To reveal the energy-dependent difference between τ_R^{left} and τ_R^{right} more intuitively, we show the stereo RABITT time delay (SRTD)

$$\tau_{SRTD} = \tau_R^{left} - \tau_R^{right}. \tag{10}$$

Note that in previous studies [40,52,53] it was assumed that the CC time delay is equal for the left and right photoelectrons and thus the SRTD is the same as the SWTD.

Figure 3 displays the SRTDs in photoemission for (Z_L, Z_R) changing from (0.0,1.0) to (0.5,0.5). For the atom $[(Z_L, Z_R) = (0.0, 1.0)]$ and the homonuclear diatomic molecule $[(Z_L, Z_R) = (0.5, 0.5)]$, τ_{SRTD} remains zero, as shown in Fig. 3. In contrast, for heteronuclear molecules, τ_{SRTD} changes its sign the increasing photoelectron energy, in agreement with the calculation results of H_2O in [61]. More interestingly, a dip around 18 eV appears in τ_{SRTD} for asymmetric molecules, as shown in Fig. 3. As the asymmetry degree of molecules decreases, this dip becomes deeper.

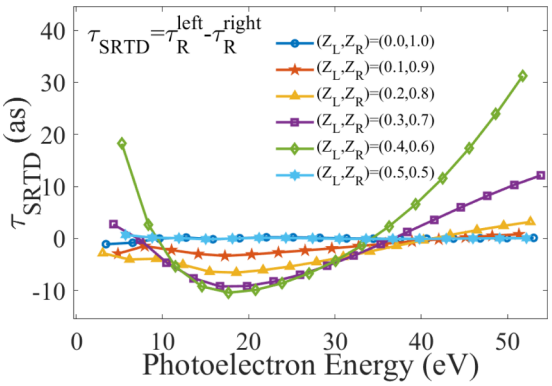

FIG. 3. The SRTDs in photoionization of different targets with nuclear charges of $(Z_L, Z_R) = (0.0, 1.0)$ (blue circles), (0.1,0.9) (orange pentagrams), (0.2,0.8) (yellow triangles), (0.3,0.7) (purple squares), (0.4,0.6) (green rhombuses), and (0.5,0.5) (sky blue hexagrams).

B. Wigner time delay

In order to reveal the origin of the oscillation occurring in the SRTD, we calculate the Wigner time delay with the SCWF method [58], as described in Sec. II C. Figures 4(a)–4(f) show the scattering phases calculated by the SCWF method, where η^{left} and η^{right} represent the scattering phases of photoelectrons emitted to the left and right sides of the target, respectively. Here the target nuclear charges (Z_L, Z_R) range from (0.0,1.0) to (0.5,0.5). In Figs. 4(a)–4(f), η^{left} rises and η^{right} declines with increasing photoelectron energy, owing to the fact that our reference atom is located between the two molecular nuclei. For the atom $[(Z_L, Z_R) = (0.0, 1.0)]$, η^{left} and η^{right} smoothly change as a function of photoelectron energy, as given in Fig. 4(a). For the molecules, as shown in Figs. 4(b)–4(f), steplike structures appear in η^{left} and η^{right}. These steps in the scattering phases become more steep as the asymmetry degree of molecules declines. For the homonuclear molecule $[(Z_L, Z_R) = (0.5, 0.5)]$, sudden phase jumps of π appear.

We calculate the Wigner time delay using the finite-difference approximation in Eq. (8), as given in Fig. 5. Here τ_W^{left} and τ_W^{right} refer to the Wigner time delays of photoelectrons emitted to the left and right, respectively. For asymmetric molecules, as displayed in Figs. 5(b)–5(e), humps appear at the energies where phase jumps happen. The width and the height of these humps depend on the asymmetry

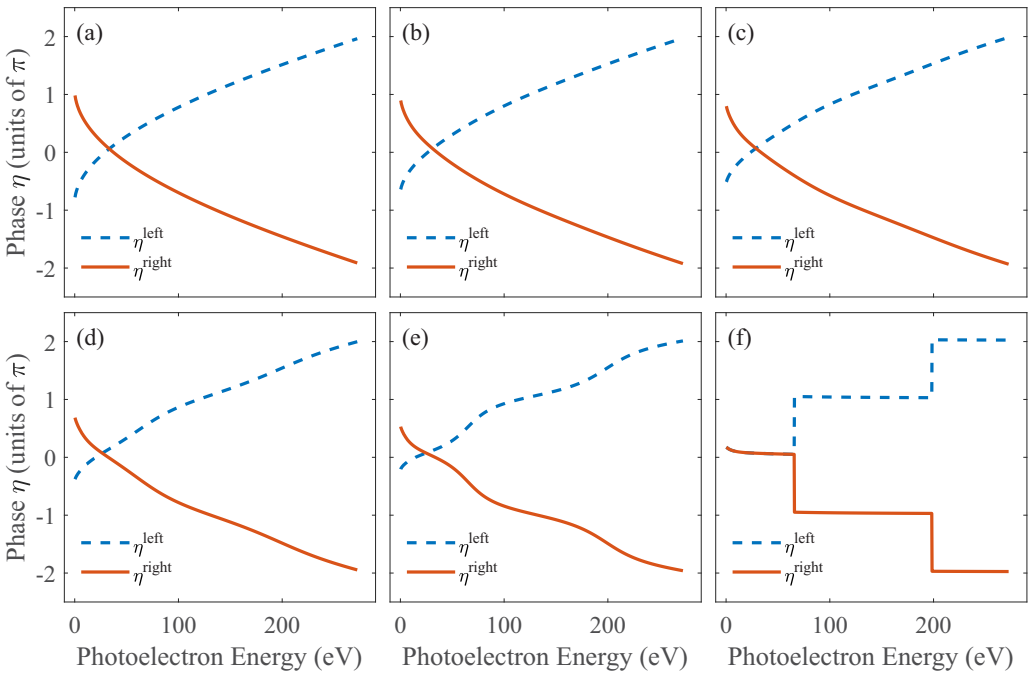

FIG. 4. Scattering phases, calculated by the SCWF method, in photoionization of different targets with nuclear charges of (a) $(Z_L, Z_R) = (0.0, 1.0)$, (b) $(Z_L, Z_R) = (0.1, 0.9)$, (c) $(Z_L, Z_R) = (0.2, 0.8)$, (d) $(Z_L, Z_R) = (0.3, 0.7)$, (e) $(Z_L, Z_R) = (0.4, 0.6)$, and (f) $(Z_L, Z_R) = (0.5, 0.5)$. The blue dashed lines are the scattering phases of photoelectrons emitted to the left and the orange solid lines correspond to photoelectrons emitted to the right.

degree of molecules. For the symmetric molecule [$(Z_L, Z_R) = (0.5, 0.5)$], the Wigner time delays are exactly the same for photoelectrons emitted to the left and right, except for the energies near the interference minima, where the absolute values of τ_W^{left} and τ_W^{right} are greatly enhanced [56].

In the following we use a two-center interference model to illustrate the mechanism of the scattering phase jumps in Fig. 4. In this model, the detected PEWP is the superposition of two waves launching from both nuclei of diatomic molecules. Here we adopt the local momentum from the

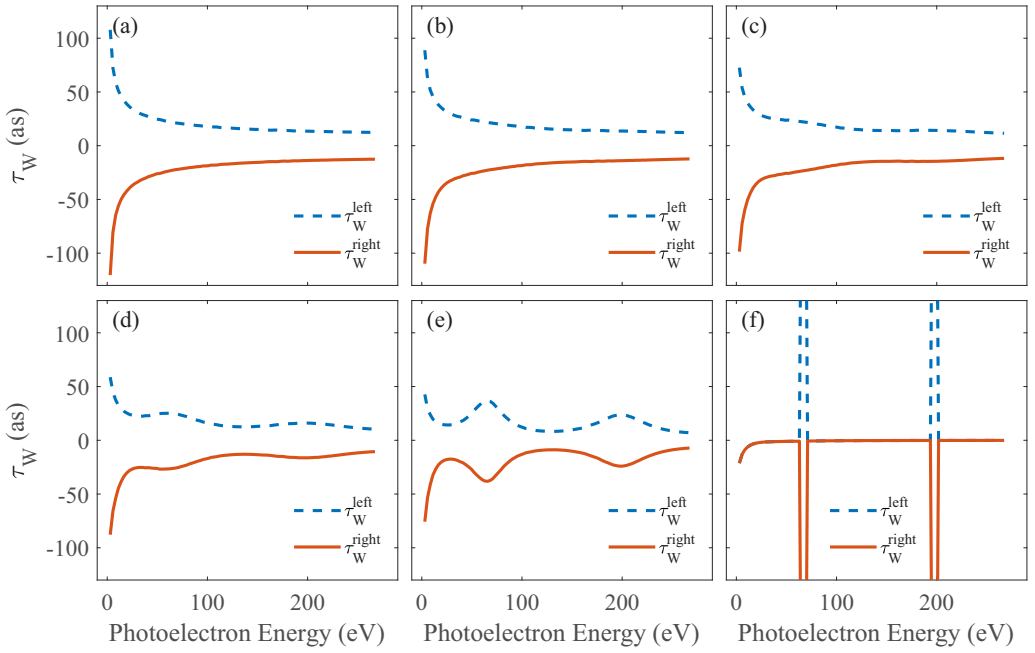

FIG. 5. Wigner time delays, calculated by the SCWF method, in photoionization of different targets with nuclear charges of (a) $(Z_L, Z_R) = (0.0, 1.0)$, (b) $(Z_L, Z_R) = (0.1, 0.9)$, (c) $(Z_L, Z_R) = (0.2, 0.8)$, (d) $(Z_L, Z_R) = (0.3, 0.7)$, (e) $(Z_L, Z_R) = (0.4, 0.6)$, and (f) $(Z_L, Z_R) = (0.5, 0.5)$. The blue dashed lines are the Wigner time delays of photoelectrons emitted to the left and the orange solid lines correspond to photoelectrons emitted to the right.

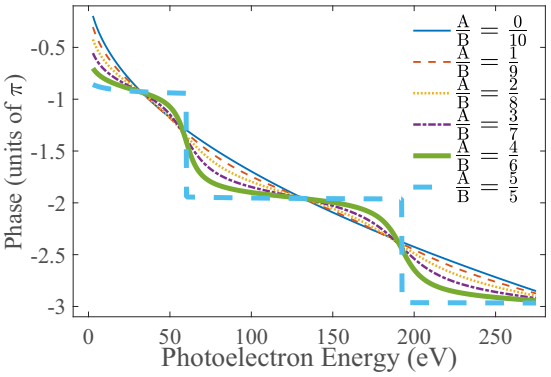

FIG. 6. Relative phases of the PEWP ψ corresponding to photoelectrons emitted to the right side, which is the superposition of two waves launching from two molecular nuclei with their amplitude ratios of $\frac{A}{B} = \frac{0}{10}$ (blue thin solid line), $\frac{1}{9}$ (orange thin dashed line), $\frac{2}{8}$ (yellow dotted line), $\frac{3}{7}$ (purple dash-dotted line), $\frac{4}{6}$ (green thick solid line), and $\frac{5}{5}$ (sky blue thick dashed line).

Wentzel-Kramers-Brillouin theory [62], and thus the wave vector is written as $k(x) = \sqrt{2[E - V(x)]}$, where E is the asymptotic energy of the photoelectrons and $V(x)$ is the molecular potential. Then the detected PEWP is described as

$$\psi = A \exp\left(i \int_{-R_0/2}^{+\infty} k(x)dx\right) + B \exp\left(i \int_{R_0/2}^{+\infty} k(x)dx\right), \tag{11}$$

where R_0 is the nuclear distance of the diatomic molecule. In Eq. (11), the parameters A and B represent the amplitudes of the photoelectron wave packets launching from two molecular nuclei. The relative values of A and B depend on the asymmetry degree of molecules. For the case $(Z_L, Z_R) = (0.0, 1.0)$, $A = 0$. For the symmetric molecule $[(Z_L, Z_R) = (0.5, 0.5)]$, $A = B$.

We calculate the phase of ψ in Eq. (11) relative to that of the photoelectron wave scattered by the reference atomic potential, for different values of $\frac{A}{B}$. Here the reference scattering phase is written as $\arg\psi_{\text{ref}} = \int_0^{+\infty} \sqrt{2[E - V_{\text{ref}}(x)]}dx$. The results are shown in Fig. 6. Here we display only the scattering phase of photoelectrons emitted to the right side. For the symmetric molecule ($A = B$), there are sudden π jumps. This is because of the familiar two-center interference for homonuclear diatomic molecules [56]. As the value of $\frac{A}{B}$ changes, the scattering phases exhibit steplike structures around two-center interference minima. The slopes of these steplike structures depend on the amplitude ratio of two waves ($\frac{A}{B}$) and thus the asymmetry degree of diatomic molecules. This behavior is the same as that in Fig. 4. Therefore, we conclude that these scattering phase jumps could be understood by the two-center interference in photoionization of diatomic molecules.

To understand the dips appearing in the SRTD in Fig. 3, we calculate the SWTD with Eq. (9) using the data in Fig. 5. The results are shown in Fig. 7, where (Z_L, Z_R) ranges from (0.0,1.0) to (0.4,0.6). For the asymmetric diatomic molecules $[(Z_L, Z_R) = (0.1, 0.9) \sim (0.4, 0.6)]$, the SWTD fluctuates as a function of photoelectron energy. There are two dips located around energies of 20 and 130 eV, respectively. The depth of these dips increases as the asymmetry degree decreases. The

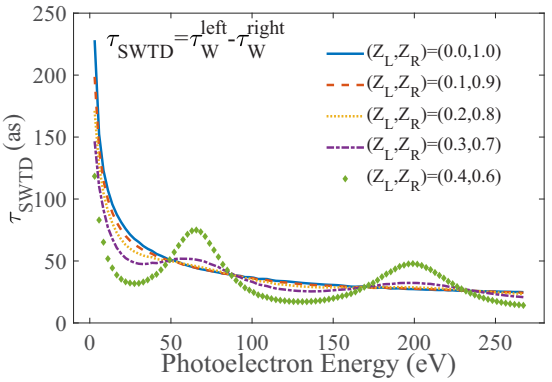

FIG. 7. The SWTDs in photoionization of different targets with nuclear charges of $(Z_L, Z_R) = (0.0, 1.0)$ (blue solid line), (0.1,0.9) (orange dashed line), (0.2,0.8) (yellow dotted line), (0.3,0.7) (purple dash-dotted line), and (0.4,0.6) (green rhombuses).

location of the first dip and its asymmetry-degree dependence are the same as those of the SRTD in Fig. 3. This indicates that the fluctuation behavior of SRTDs originates from the oscillating Wigner time delays, which is associated with two-center interferences.

For the atom $(Z_L, Z_R) = (0.0, 1.0)$, the SWTD decreases monotonically. In this case, it has been illustrated that the SWTD is associated with the launching position of the ionized electron wave packet according to [40]

$$\tau_{\langle \text{SW} \rangle} = \frac{2x_0}{\sqrt{2E}}, \tag{12}$$

where E is the asymptotic energy of the photoelectrons and x_0 is the mean position of electrons at the moment of birth with respect to the reference center (in our case the reference center is located at $x = 0$ a.u., and $x_0 = 2.0$ a.u.). Figure 8 displays $\tau_{\langle \text{SW} \rangle}$ calculated with Eq. (12). In Fig. 8, $\tau_{\langle \text{SW} \rangle}$ and τ_{SWTD} are in excellent agreement for the atom case $[(Z_L, Z_R) = (0.0, 1.0)]$, which verifies that the SWTD could be interpreted by the shifted mean position of electrons at the moment of birth, as proposed in [40].

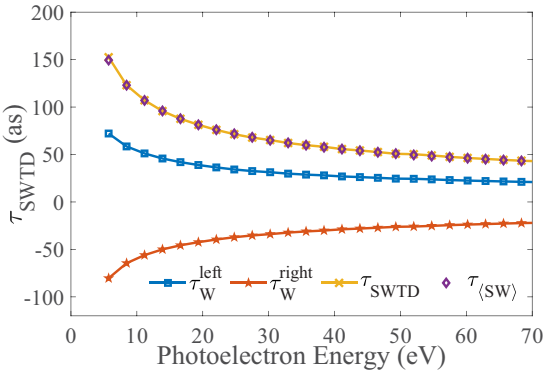

FIG. 8. The SWTD [Eq. (9), yellow crosses], the mean SWTD [Eq. (12), purple rhombuses], and the Wigner time delays in photoionization of the atom $[(Z_L, Z_R) = (0.0, 1.0)]$. The blue squares are the Wigner time delay of photoelectrons emitted to the left and the orange pentagrams correspond to photoelectrons emitted to the right.

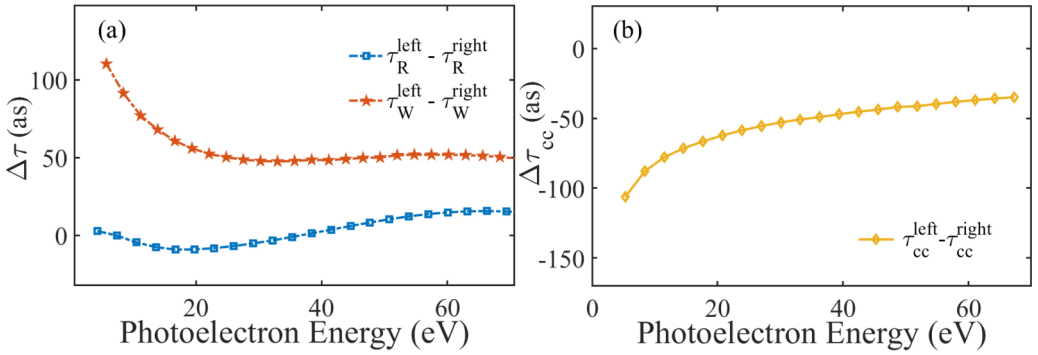

FIG. 9. (a) The SRTD (blue squares) and the SWTD (orange pentagrams) in photoionization of the asymmetric diatomic molecule $[(Z_L, Z_R) = (0.3, 0.7)]$. (b) Left-right relative CC time delay (yellow rhombuses) in photoionization for the asymmetric diatomic molecule $[(Z_L, Z_R) = (0.3, 0.7)]$.

For the cases of diatomic molecules, electron wave packets launch from both nuclei and thus the picture above breaks down. Instead, the interference between the two wave packets from different nuclei should be considered. It leads to the fluctuation in the SWTD and thus the SRTD, as given in Figs. 3 and 7.

C. Continuum-continuum time delay

The time delay in RABITT measurements, τ_R, can be decomposed into the Wigner time delay τ_W and the CC time delay τ_{CC}, according to Eq. (5). Here τ_W, the term of most interest, is expected to be extracted directly from RABITT measurements. In previous studies, τ_{CC} was thought to be a universal quantity owing to the symmetric contribution of the long-range Coulomb potential [26]. Therefore, τ_{CC} is removed from the stereo measurement [40,52,53] and thus the SWTD [Eq. (9)] equals the SRTD [Eq. (10)].

However, in our work, the SWTD is not the same as the SRTD for asymmetric molecules. The SRTDs shown in Fig. 3 oscillate around zero for asymmetric molecules, while the SWTDs given in Fig. 7 remain positive. To reveal the difference between the SWTD and the SRTD for asymmetric molecules more clearly, we display the SRTD and the SWTD for the molecule $(Z_L, Z_R) = (0.3, 0.7)$ in Fig. 9(a). The obvious difference between the SRTD and the SWTD, as displayed in Fig. 9(a), indicates that the CC time delay is left-right asymmetric in photoemission of asymmetric molecules. The relative left-right CC time delay $(\tau_{CC}^{left} - \tau_{CC}^{right})$ for the molecule $(Z_L, Z_R) = (0.3, 0.7)$ is shown in Fig. 9(b). This relative CC time delay is large at low energies, up to 100 as. As the photoelectron energy increases, the difference between the left-right CC time delays τ_{CC}^{left} and τ_{CC}^{right} becomes smaller.

Note that the time delay in RABITT measurements is independent of where the reference center is located, while the reference center's position affects the Wigner time delay and thus the CC time delay. In our calculation, the reference center is placed at $x = 0$ a.u.

In previous theories, the analytic expression of τ_{CC} was derived by applying the asymptotic approximation in the lowest-order perturbation theory [26,27]. This analytic expression indicates that τ_{CC} is universal, only depending on the momenta of two continuum states in the two-photon transition and the ionic Coulomb potential [26]. However, recent calculations and experiments demonstrated that the actual CC time delay is nonuniversal [27]. It depends on angular momenta [30,44,63] and is heavily influenced by the partial wave interference characteristic [64]. The angular momentum dependence of τ_{CC} is attributed to the centrifugal-potential effect on the scattering phase in CC transitions [44]. For asymmetric molecules, the CC transition probes the potential landscape at large distances where the potential $\sim\frac{1}{r^2}$ (which is anisotropic for the asymmetric molecular potential) is non-negligible. Therefore, the CC time delay in photoionization of asymmetric molecules depends on the emission direction of photoelectrons.

IV. CONCLUSION

We have calculated the time delay of diatomic molecules in reconstruction of attosecond beating by interference of two-photon transitions (RABITT) measurements by solving the time-dependent Schrödinger equation (TDSE). Our results show that for asymmetric diatomic molecules, the stereo RABITT time delay (SRTD) fluctuates as a function of photoelectron energy. This fluctuation is due to the oscillating stereo Wigner time delay (SWTD), which is traced to the interference between the electron wave packets launching from two molecular nuclei. For extremely asymmetric diatomic molecules, the electron wave packet predominantly launches from one nucleus of the molecule and thus the interference effect is negligible. In this case, the SWTD could be interpreted by the shifted mean position of electrons at the moment of birth. Furthermore, for asymmetric diatomic molecules, there is a difference between the SWTD and the SRTD, which reveals the left-right difference of the continuum-continuum (CC) time delays. This asymmetric CC time delay indicates that the CC transition probes part of the $\sim\frac{1}{r^2}$ potential landscape, which is anisotropic for the heteronuclear molecular potential.

Our one-dimensional model shows a dip in the stereo time delay in the photoionization of heteronuclear molecules. We believe this dip exists in full-dimensional calculations and is experimentally observable. Moreover, in real molecules, multielectron effects and the nuclear motion may affect the details of the stereo time delay, which requires more sophisticated studies.

ACKNOWLEDGMENTS

The authors acknowledge stimulating discussions with Professor Manfred Lein and Dr. Tomáš Zimmermann. This work was supported by National Key Research and Development Program of China (Grant No. 2019YFA0308300), National Natural Science Foundation of China (Grants No. 11874163 and No. 12021004), and Chinese Academy of Sciences (Grants No. J19-121-III and No. S19-001).

[1] M. Hentschel, R. Kienberger, C. Spielmann, G. A. Reider, N. Milosevic, T. Brabec, P. Corkum, U. Heinzmann, M. Drescher, and F. Krausz, Nature (London) **414**, 509 (2001).

[2] P. M. Paul, E. S. Toma, P. Breger, G. Mullot, F. Augé, P. Balcou, H. G. Muller, and P. Agostini, Science **292**, 1689 (2001).

[3] M. Drescher, M. Hentschel, R. Kienberger, G. Tempea, C. Spielmann, G. A. Reider, P. B. Corkum, and F. Krausz, Science **291**, 1923 (2001).

[4] R. Kienberger, E. Goulielmakis, M. Uiberacker, A. Baltuska, V. Yakovlev, F. Bammer, A. Scrinzi, T. Westerwalbesloh, U. Kleineberg, U. Heinzmann, M. Drescher, and F. Krausz, Nature (London) **427**, 817 (2004).

[5] G. Sansone, E. Benedetti, F. Calegari, C. Vozzi, L. Avaldi, R. Flammini, L. Poletto, P. Villoresi, C. Altucci, R. Velotta, S. Stagira, S. De Silvestri, and M. Nisoli, Science **314**, 443 (2006).

[6] A. L. Cavalieri, N. Müller, T. Uphues, V. S. Yakovlev, A. Baltuška, B. Horvath, B. Schmidt, L. Blümel, R. Holzwarth, S. Hendel, M. Drescher, U. Kleineberg, P. M. Echenique, R. Kienberger, F. Krausz, and U. Heinzmann, Nature (London) **449**, 1029 (2007).

[7] M. Sabbar, S. Heuser, R. Boge, M. Lucchini, T. Carette, E. Lindroth, L. Gallmann, C. Cirelli, and U. Keller, Phys. Rev. Lett. **115**, 133001 (2015).

[8] J. Mauritsson, M. B. Gaarde, and K. J. Schafer, Phys. Rev. A **72**, 013401 (2005).

[9] M. Swoboda, T. Fordell, K. Klünder, J. M. Dahlström, M. Miranda, C. Buth, K. J. Schafer, J. Mauritsson, A. L'Huillier, and M. Gisselbrecht, Phys. Rev. Lett. **104**, 103003 (2010).

[10] D. Guénot, D. Kroon, E. Balogh, E. W. Larsen, M. Kotur, M. Miranda, T. Fordell, P. Johnsson, J. Mauritsson, M. Gisselbrecht, K. Varjù, C. L. Arnold, T. Carette, A. S. Kheifets, E. Lindroth, A. L'Huillier, and J. M. Dahlström, J. Phys. B **47**, 245602 (2014).

[11] C. Palatchi, J. M. Dahlström, A. S. Kheifets, I. A. Ivanov, D. M. Canaday, P. Agostini, and L. F. DiMauro, J. Phys. B **47**, 245003 (2014).

[12] E. S. Toma and H. G. Muller, J. Phys. B **35**, 3435 (2002).

[13] R. Pazourek, S. Nagele, and J. Burgdörfer, Rev. Mod. Phys. **87**, 765 (2015).

[14] A. W. Bray, F. Naseem, and A. S. Kheifets, Phys. Rev. A **97**, 063404 (2018).

[15] D. Guénot, K. Klünder, C. L. Arnold, D. Kroon, J. M. Dahlström, M. Miranda, T. Fordell, M. Gisselbrecht, P. Johnsson, J. Mauritsson, E. Lindroth, A. Maquet, R. Taïeb, A. L'Huillier, and A. S. Kheifets, Phys. Rev. A **85**, 053424 (2012).

[16] V. Gruson, L. Barreau, Á. Jiménez-Galan, F. Risoud, J. Caillat, A. Maquet, B. Carré, F. Lepetit, J.-F. Hergott, T. Ruchon, L. Argenti, R. Taïeb, F. Martín, and P. Salières, Science **354**, 734 (2016).

[17] W. Boutu, S. Haessler, H. Merdji, P. Breger, G. Waters, M. Stankiewicz, L. J. Frasinski, R. Taïeb, J. Caillat, A. Maquet, P. Monchicourt, B. Carre, and P. Salieres, Nat. Phys. **4**, 545 (2008).

[18] M. Huppert, I. Jordan, D. Baykusheva, A. von Conta, and H. J. Wörner, Phys. Rev. Lett. **117**, 093001 (2016).

[19] S. Haessler, B. Fabre, J. Higuet, J. Caillat, T. Ruchon, P. Breger, B. Carré, E. Constant, A. Maquet, E. Mével, P. Salières, R. Taïeb, and Y. Mairesse, Phys. Rev. A **80**, 011404(R) (2009).

[20] L. Cattaneo, J. Vos, R. Y. Bello, A. Palacios, S. Heuser, L. Pedrelli, M. Lucchini, C. Cirelli, F. Martín, and U. Keller, Nat. Phys. **14**, 733 (2018).

[21] M. J. Ambrosio and U. Thumm, Phys. Rev. A **94**, 063424 (2016).

[22] M. Lucchini, L. Castiglioni, L. Kasmi, P. Kliuiev, A. Ludwig, M. Greif, J. Osterwalder, M. Hengsberger, L. Gallmann, and U. Keller, Phys. Rev. Lett. **115**, 137401 (2015).

[23] R. Locher, L. Castiglioni, M. Lucchini, M. Greif, L. Gallmann, J. Osterwalder, M. Hengsberger, and U. Keller, Optica **2**, 405 (2015).

[24] J. M. Dahlström, A. L'Huillier, and A. Maquet, J. Phys. B **45**, 183001 (2012).

[25] A. Maquet, J. Caillat, and R. Taïeb, J. Phys. B **47**, 204004 (2014).

[26] J. Dahlström, D. Guénot, K. Klünder, M. Gisselbrecht, J. Mauritsson, A. L'Huillier, A. Maquet, and R. Taïeb, Chem. Phys. **414**, 53 (2013).

[27] D. Baykusheva and H. J. Wörner, J. Chem. Phys. **146**, 124306 (2017).

[28] P. Hockett, E. Frumker, D. M. Villeneuve, and P. B. Corkum, J. Phys. B **49**, 095602 (2016).

[29] L. Argenti, A. Jiménez-Galán, J. Caillat, R. Taïeb, A. Maquet, and F. Martín, Phys. Rev. A **95**, 043426 (2017).

[30] D. Bharti, D. Atri-Schuller, G. Menning, K. R. Hamilton, R. Moshammer, T. Pfeifer, N. Douguet, K. Bartschat, and A. Harth, Phys. Rev. A **103**, 022834 (2021).

[31] A. Jiménez-Galán, F. Martín, and L. Argenti, Phys. Rev. A **93**, 023429 (2016).

[32] E. P. Wigner, Phys. Rev. **98**, 145 (1955).

[33] F. T. Smith, Phys. Rev. **118**, 349 (1960).

[34] M. Schultze, M. Fieß, N. Karpowicz, J. Gagnon, M. Korbman, M. Hofstetter, S. Neppl, A. L. Cavalieri, Y. Komninos, T. Mercouris, C. A. Nicolaides, R. Pazourek, S. Nagele, J. Feist, J. Burgdörfer, A. M. Azzeer, R. Ernstorfer, R. Kienberger, U. Kleineberg, E. Goulielmakis *et al.*, Science **328**, 1658 (2010).

[35] K. Klünder, J. M. Dahlström, M. Gisselbrecht, T. Fordell, M. Swoboda, D. Guénot, P. Johnsson, J. Caillat, J. Mauritsson, A. Maquet, R. Taïeb, and A. L'Huillier, Phys. Rev. Lett. **106**, 143002 (2011).

[36] M. Isinger, R. J. Squibb, D. Busto, S. Zhong, A. Harth, D. Kroon, S. Nandi, C. L. Arnold, M. Miranda, J. M. Dahlström, E. Lindroth, R. Feifel, M. Gisselbrecht, and A. L'Huillier, Science **358**, 893 (2017).

[37] S. Heuser, A. Jiménez Galán, C. Cirelli, C. Marante, M. Sabbar, R. Boge, M. Lucchini, L. Gallmann, I. Ivanov, A. S. Kheifets, J. M. Dahlström, E. Lindroth, L. Argenti, F. Martín, and U. Keller, Phys. Rev. A **94**, 063409 (2016).

[38] C. Cirelli, C. Marante, S. Heuser, C. L. M. Petersson, Á. J. Galán, L. Argenti, S. Zhong, D. Busto, M. Isinger, S. Nandi, S. Maclot, L. Rading, P. Johnsson, M. Gisselbrecht, M. Lucchini, L. Gallmann, J. M. Dahlström, E. Lindroth, A. L'Huillier, F. Martín *et al.*, Nat. Commun. **9**, 955 (2018).

[39] P. Hockett, J. Phys. B **50**, 154002 (2017).

[40] J. Vos, L. Cattaneo, S. Patchkovskii, T. Zimmermann, C. Cirelli, M. Lucchini, A. Kheifets, A. S. Landsman, and U. Keller, Science **360**, 1326 (2018).

[41] J. Caillat, A. Maquet, S. Haessler, B. Fabre, T. Ruchon, P. Salières, Y. Mairesse, and R. Taïeb, Phys. Rev. Lett. **106**, 093002 (2011).

[42] S. Biswas, B. Förg, L. Ortmann, J. Schötz, W. Schweinberger, T. Zimmermann, L. Pi, D. Baykusheva, H. A. Masood, I. Liontos, A. M. Kamal, N. G. Kling, A. F. Alharbi, M. Alharbi, A. M. Azzeer, G. Hartmann, H. J. Wörner, A. S. Landsman, and M. F. Kling, Nat. Phys. **16**, 778 (2020).

[43] S. Beaulieu, A. Comby, A. Clergerie, J. Caillat, D. Descamps, N. Dudovich, B. Fabre, R. Géneaux, F. Légaré, S. Petit, B. Pons, G. Porat, T. Ruchon, R. Taïeb, V. Blanchet, and Y. Mairesse, Science **358**, 1288 (2017).

[44] J. Fuchs, N. Douguet, S. Donsa, F. Martin, J. Burgdörfer, L. Argenti, L. Cattaneo, and U. Keller, Optica **7**, 154 (2020).

[45] L.-W. Pi and A. S. Landsman, Applied Sciences **8**, 322 (2018).

[46] C. Alexandridi, D. Platzer, L. Barreau, D. Busto, S. Zhong, M. Turconi, L. Neoričić, H. Laurell, C. L. Arnold, A. Borot, J.-F. Hergott, O. Tcherbakoff, M. Lejman, M. Gisselbrecht, E. Lindroth, A. L'Huillier, J. M. Dahlström, and P. Salières, Phys. Rev. Research **3**, L012012 (2021).

[47] D. Hammerland, P. Zhang, A. Bray, C. F. Perry, S. Kuehn, P. Jojart, I. Seres, V. Zuba, Z. Varallyay, K. Osvay, A. Kheifets, T. T. Luu, and H. J. Woerner, arXiv:1907.01219.

[48] M. Ossiander, F. Siegrist, V. Shirvanyan, R. Pazourek, A. Sommer, T. Latka, A. Guggenmos, S. Nagele, J. Feist, J. Burgdörfer, R. Kienberger, and M. Schultze, Nat. Phys. **13**, 280 (2017).

[49] C. Lemell, B. Solleder, K. Tőkési, and J. Burgdörfer, Phys. Rev. A **79**, 062901 (2009).

[50] A. K. Kazansky and P. M. Echenique, Phys. Rev. Lett. **102**, 177401 (2009).

[51] C.-H. Zhang and U. Thumm, Phys. Rev. Lett. **102**, 123601 (2009).

[52] A. Chacon, M. Lein, and C. Ruiz, Phys. Rev. A **89**, 053427 (2014).

[53] A. Chacón and C. Ruiz, Opt. Express **26**, 4548 (2018).

[54] H. D. Cohen and U. Fano, Phys. Rev. **150**, 30 (1966).

[55] V. V. Serov, V. L. Derbov, and T. A. Sergeeva, Phys. Rev. A **87**, 063414 (2013).

[56] Q.-C. Ning, L.-Y. Peng, S.-N. Song, W.-C. Jiang, S. Nagele, R. Pazourek, J. Burgdörfer, and Q. Gong, Phys. Rev. A **90**, 013423 (2014).

[57] V. V. Serov and A. S. Kheifets, Phys. Rev. A **93**, 063417 (2016).

[58] R. Gaillac, M. Vacher, A. Maquet, R. Taïeb, and J. Caillat, Phys. Rev. A **93**, 013410 (2016).

[59] M. Feit, J. Fleck, and A. Steiger, J. Comput. Phys. **47**, 412 (1982).

[60] A. Messiah, *Quantum Mechanics: Two Volumes Bound as One* (Dover, Mineola, 2014).

[61] V. V. Serov and A. S. Kheifets, J. Chem. Phys. **147**, 204303 (2017).

[62] H. Friedrich, *Theoretical Atomic Physics* (Springer, Berlin, 1991).

[63] I. A. Ivanov and A. S. Kheifets, Phys. Rev. A **96**, 013408 (2017).

[64] S. Donsa, M. Ederer, R. Pazourek, J. Burgdörfer, and I. Březinová, Phys. Rev. A **102**, 033112 (2020).